Open access • Journal Article • DOI:10.1103/PHYSREVE.57.1563

Frequency locking in Josephson arrays: Connection with the Kuramoto model

Kurt Wiesenfeld, Pere Colet, Steven H. Strogatz

Institutions: Georgia Institute of Technology, Spanish National Research Council, Cornell University

Published on: 01 Feb 1998 - Physical Review E (American Physical Society)

Topics: Kuramoto model and Josephson effect

Frequency locking in Josephson arrays: Connection with the Kuramoto model

Kurt Wiesenfeld
School of Physics, Georgia Institute of Technology, Atlanta, Georgia 30332

Pere Colet
Instituto Mediterraneo de Estudios Avanzados (CSIC-UIB), E-07071 Palma de Mallorca, Spain

Steven H. Strogatz
Theoretical and Applied Mechanics, Kimball Hall, Cornell University, Ithaca, New York 14853
(Received 1 July 1997)

The circuit equations for certain series arrays of Josephson junctions can be mapped onto a simple model originally introduced by Kuramoto [in *Proceedings of the International Symposium on Mathematical Problems in Theoretical Physics*, edited by H. Araki, Lecture Notes in Physics Vol. 39 (Springer, Berlin, 1975)] to study fundamental aspects of frequency locking in large populations of nonlinear oscillators. This correspondence makes it possible to derive accurate theoretical predictions of transitions signaling the onset of partial and complete locking, respectively. We calculate that both transitions should be observable experimentally using present fabrication tolerances. [S1063-651X(98)06102-9]

PACS number(s): 05.45.+b, 74.50.+r, 74.40.+k

I. INTRODUCTION

Josephson junction arrays are of interest for a variety of reasons, both fundamental and applied [1–4]. On the fundamental side they have been used to study two-dimensional melting, flux creep in type-II superconductors, and the nonlinear dynamics of coupled oscillators [5]. Josephson arrays are presently used to maintain the U.S. Legal Volt [6], and researchers are pursuing applications where arrays could be used as sensitive parametric amplifiers [7] and tunable local oscillators [8] at millimeter and submillimeter wavelengths.

This last application directly overlaps with a particular fundamental topic drawn from the field of nonlinear dynamics, namely, mutual synchronization. It is well known that populations of coupled nonlinear oscillators can spontaneously synchronize to a common frequency, despite differences in their natural frequencies. This phenomenon has been observed in many physical and biological systems, including relaxation oscillator circuits, networks of neurons and cardiac pacemaker cells, chorusing crickets, and fireflies that flash in unison [9,10]. The first systematic experimental study was performed in 1665 by Huygens with two marine pendulum clocks hanging from a common support [11].

In a pioneering study, Winfree [12] developed a mathematical framework for studying large populations of limit-cycle oscillators and showed that the onset of synchronization is analogous to a thermodynamic phase transition. This observation was refined by Kuramoto [13], who proposed and analyzed an exactly solvable mean-field model of coupled oscillators with distributed natural frequencies. The Kuramoto model has stimulated much theoretical work [14–22], thanks to its analytical tractability.

In this paper we show how the lump circuit equations for a series array of zero-capacitance Josephson junctions can be mapped onto the Kuramoto model in the limit of weak coupling and weak disorder. This allows us to answer the question how large a spread in the junction parameters can be tolerated if the array is to achieve perfect frequency locking. In fact, we can analytically determine the fraction of junctions that frequency lock as a function of the various circuit parameters. The Josephson array can display two transitions: The first corresponds to the onset of dynamical order, the second coincides with complete frequency locking. We find that both transitions should be experimentally accessible with existing technology.

In Sec. II we review both the lump circuit model for Josephson series arrays and the Kuramoto model for coupled oscillators. Section III establishes the connection between the two models. The analytical results known for the Kuramoto model are summarized in Sec. IV and then used in Sec. V to predict the synchronization properties of Josephson arrays. We show that these predictions are in good agreement with numerical simulations of the full equations for the lump circuit. Some of the work reported here was presented earlier in abbreviated form [23].

II. BACKGROUND

Consider a series array of N junctions, biased with a constant current I_B and subject to a load with inductance L, resistance R, and capacitance C (Fig. 1). For junctions with negligible capacitance, the governing circuit equations are [24]

$$\frac{\hbar}{2er_j}\dot{\phi}_j + I_j \sin\phi_j + \dot{Q} = I_B, \quad j = 1, \ldots, N \tag{1}$$

$$L\ddot{Q} + R\dot{Q} + \frac{1}{C}Q = \frac{\hbar}{2e}\sum_{k=1}^{N} \dot{\phi}_k, \tag{2}$$

where ϕ_j is the wave-function phase difference across the jth Josephson junction, r_j is the junction resistance, I_j is the

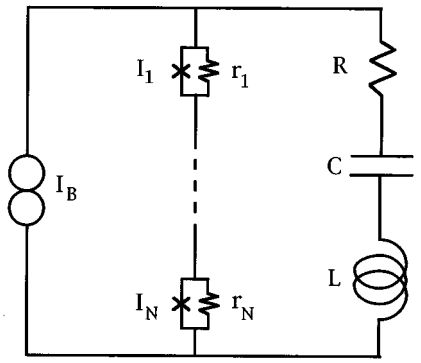

FIG. 1. Circuit model for a current biased series array of Josephson junctions shunted in parallel by an inductor-capacitor-resistor load.

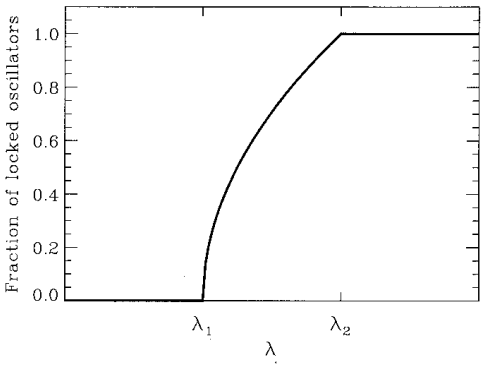

FIG. 2. Typical behavior of the fraction of frequency locked oscillators f as a function of coupling strength λ.

junction critical current, Q is the charge on the load capacitor, $\hbar$ is Planck's constant divided by 2π, and e is the elementary charge. The overdot denotes differentiation with respect to time. The voltage drop across the jth junction is $(\hbar/2e)\dot{\phi}_j$.

Equation (1) shows that the coupling between the junctions is mediated by the load current $\dot{Q}$. In the absence of a load the junctions are dynamically uncoupled and (for $I_B > I_j$) the jth element executes voltage oscillations at its bare frequency

$$\omega_j = \frac{2er_j}{\hbar}(I_B^2 - I_j^2)^{1/2}. \tag{3}$$

The load causes the elements to oscillate at shifted frequencies $\{\tilde{\omega}_j\}$, making it possible for junctions with different bare frequencies $\{\omega_j\}$ to oscillate at a common frequency Ω. This requires the coupling to be large enough to overcome the intrinsic spread in the bare frequencies; the larger the coupling, the greater the number of elements entrained.

Our goal is to calculate, as a function of the various system parameters, the fraction of junctions that become perfectly frequency locked. We also want to calculate the total power generated at the locking frequency Ω, a quantity that also involves the relative phases of the locked elements. We can achieve these goals by mapping Eqs. (1) and (2) onto the Kuramoto-Sakaguchi model [15] for a set of N globally coupled limit-cycle oscillators

$$\dot{\theta}_j = \omega_j - \frac{K}{N}\sum_{k=1}^{N} \sin(\theta_j - \theta_k + \alpha) \tag{4}$$

for $j = 1, \ldots, N$, where θ_j is the phase of the jth oscillator, ω_j is its bare frequency, K is the coupling constant, and α is a constant whose role is discussed below. The Kuramoto-Sakaguchi model can be solved in the large-N limit using a self-consistency approach. In Sec. III we derive Eq. (4) from the Josephson circuit equations, in the limit of weak disorder and weak coupling; the quantitative consequences for the dynamics of the Josephson array are tackled in the following sections. The remainder of this section is devoted to a summary of the qualitative picture that emerges from that analysis.

The essence of the problem is the competition between the intrinsic disorder (i.e., variations in the junction resistances and critical currents) and the dynamical coupling strength. In the Kuramoto model, the disorder enters via the distribution of natural frequencies, while the effective coupling strength is set by the parameter combination $\lambda = K\cos\alpha$. If $\lambda > 0$ then the coupling is ''attractive'' and tends to induce frequency locking. As λ is decreased from a large positive value, three dynamical regimes are encountered, as shown in Fig. 2. For $\lambda > \lambda_2$ all of the oscillators are frequency locked, for $\lambda_2 > \lambda > \lambda_1$ some finite fraction is locked, and for $\lambda_1 > \lambda$ there is no frequency locking.

In the Josephson junction array, one does not have independent control over the parameters appearing in Eq. (4). For example, the most natural control parameter is the bias current I_B and (as we shall see) varying this parameter simultaneously changes all of the quantities K, $\cos\alpha$, and the N bare frequencies $\{\omega_j\}$. Moreover, the effective coupling strength λ cannot be increased to an arbitrarily large value. As might be expected, the values of the transition points increase with increasing intrinsic disorder. Consequently, depending on the various circuit parameters, it can happen that one or both of the transition points (λ_1, λ_2) are not observed in a particular array. However, we find that complete frequency locking *should* be observable using present technology, with tolerances in the junction parameters on the order of a percent [25]. We discuss this point in Sec. V.

III. DERIVATION OF THE AVERAGED EQUATIONS

In this section we show that the Josephson system (1) and (2) can be mapped onto Kuramoto's model (4) in the limit of weak coupling and weak disorder. Our derivation is a straightforward extension of the averaging procedure previously applied to identical junction arrays [26,27].

The first step is to introduce ''natural angles'' θ_j defined by

$$\frac{2er_j}{\hbar}\frac{d\theta_j}{\omega_j} = \frac{d\phi_j}{I_B - I_j\sin\phi_j}. \tag{5}$$

The angles θ_j are natural in the sense that, in the uncoupled limit, they rotate uniformly, while the ϕ_j do not. Direct integration of this equation yields the useful trigonometric relation

$$I_B - I_j \sin\phi_j = (I_B^2 - I_j^2)/(I_B - I_j \cos\theta_j). \tag{6}$$

Thus Eq. (1) can be rewritten as

$$\dot{\theta}_j = \omega_j - \frac{\omega_j \dot{Q}}{I_B^2 - I_j^2}(I_B - I_j \cos\theta_j). \tag{7}$$

We assume that the disorder is weak, so it is convenient to write

$$r_j = \bar{r}(1 + \epsilon\rho_j), \tag{8a}$$

$$I_j = \bar{I}(1 + \epsilon\zeta_j), \tag{8b}$$

$$\omega_j = \bar{\omega}(1 + \epsilon\delta_j), \tag{8c}$$

where ϵ is a formal parameter used to keep track of small quantities and the overbar denotes a sample mean. Note that ρ_j, ζ_j, and δ_j are not independent: From Eq. (3), we see that to leading order,

$$\delta_j = \rho_j - \frac{\bar{I}}{I_B^2 - \bar{I}^2}\zeta_j + O(\epsilon).$$

In what follows we also assume that the bias current is not too close to the critical current $[I_B - I_j > O(\epsilon)]$ and that the coupling is weak $[\dot{Q} = O(\epsilon)]$. Thus Eq. (7) becomes

$$\dot{\theta}_j = \bar{\omega} + \epsilon\bar{\omega}\delta_j - \frac{\bar{\omega}\dot{Q}}{I_B^2 - \bar{I}^2}(I_B - \bar{I}\cos\theta_j) + O(\epsilon^2). \tag{9}$$

The basic idea behind the averaging method is as follows. Equation (9) shows that $\dot{\theta}_j - \bar{\omega} = O(\epsilon)$; hence $\theta_j(t) - \bar{\omega}t$ is a slowly varying quantity that changes significantly only on a long time scale $t = O(1/\epsilon)$. Hence, on the fast $O(1)$ time scale of a single oscillation, $\theta_j(t) - \bar{\omega}t$ is almost constant and may therefore be replaced by its running average over one cycle. To determine how $\theta_j(t) - \bar{\omega}t$ varies on the long time scale, we time average the right-hand side of Eq. (9) and replace $\theta_j(t)$ with $\bar{\omega}t + \theta_j(0) + O(\epsilon)$. This procedure yields an equation correct to first order for the slow evolution of $\theta_j(t) - \bar{\omega}t$. To do the calculation explicitly we need an expression for $\dot{Q}(t)$, but this is readily obtained from Eq. (2), as we now show.

To find $\dot{Q}$, note first that Eqs. (1) and (6) imply

$$\frac{\hbar}{2e}\dot{\phi}_j = \frac{I_B^2 - I_j^2}{I_B - I_j \cos\theta_j} r_j - \dot{Q} r_j, \tag{10}$$

so that Eq. (2) becomes

$$L\ddot{Q} + \left(R + \sum_k r_k\right)\dot{Q} + \frac{1}{C}Q = \sum_k r_k \frac{I_B^2 - I_k^2}{I_B - I_k \cos\theta_k}. \tag{11}$$

To leading order in ϵ,

$$L\ddot{Q} + (R + N\bar{r})\dot{Q} + \frac{1}{C}Q = \bar{r}(I_B^2 - \bar{I}^2)\sum_k \frac{1}{I_B - \bar{I}\cos[\bar{\omega}t + \theta_k(0)]}. \tag{12}$$

This is the equation for a periodically driven harmonic oscillator. For convenience, introduce the Fourier cosine series

$$\frac{1}{I_B - \bar{I}\cos(\bar{\omega}t)} = \sum_{n=0}^{\infty} A_n \cos n\bar{\omega}t \tag{13}$$

so that, for example,

$$A_1 = \frac{2}{\bar{I}}\left(\frac{I_B}{\sqrt{I_B^2 - \bar{I}^2}} - 1\right). \tag{14}$$

Then Eq. (12) has the steady-state solution

$$Q(t) = \sum_{k=1}^{N}\sum_{n=0}^{\infty} B_n \cos[n\bar{\omega}t + n\theta_k(0) + \beta_n], \tag{15}$$

where

$$B_n^2 = \frac{\bar{r}^2(I_B^2 - \bar{I}^2)^2 A_n^2}{(Ln^2\bar{\omega}^2 - 1/C)^2 + n^2\bar{\omega}^2(R + N\bar{r})^2} \tag{16}$$

and

$$\beta_n = \arctan\frac{n\bar{\omega}(R + N\bar{r})}{Ln^2\bar{\omega}^2 - 1/C}. \tag{17}$$

The relative sign between A_n and B_n determines the correct branch of the inverse tangent: One can easily check that $\sin\beta_n$ has the opposite sign of the ratio A_n/B_n and, for $\omega > 1/\sqrt{LC}$, $\cos\beta_n$ also has the opposite sign of A_n/B_n. We choose the B_n to be positive; consequently, if A_n is positive then $-\pi < \beta_n < -\pi/2$.

Having found $Q(t)$ to leading order in ϵ, we are now ready to derive the averaged equations for the phases. Substitution of expression (15) into Eq. (9) and taking the time average over one period yields

$$\dot{\theta}_j = \bar{\omega} + \epsilon\bar{\omega}\delta_j - \frac{\bar{\omega}^2\bar{I}}{I_B^2 - \bar{I}^2}\frac{B_1}{2}\sum_{k=1}^{N}\sin(\theta_k - \theta_j + \beta_1), \tag{18}$$

where $\theta_k(0) - \theta_j(0)$ has been replaced by $\theta_k(t) - \theta_j(t)$. [This replacement introduces another negligible error of $O(\epsilon^2)$ into the averaged equations.] To recast these equations into the form of the Kuramoto model, set $\alpha = -\pi - \beta_1$. Then $\sin(\theta_k - \theta_j + \beta_1) = \sin(\theta_j - \theta_k + \alpha)$. Finally, to first order in ϵ, Eq. (18) is equivalent to

$$\dot{\theta}_j = \omega_j - \frac{K}{N}\sum_{k=1}^{N}\sin(\theta_j - \theta_k + \alpha), \tag{19}$$

where, in terms of the original circuit parameters,

$$K=\frac{N\bar{r}\bar{\omega}\left(\frac{2e}{\hbar}\bar{r}I_B-\bar{\omega}\right)}{[(L\bar{\omega}^2-1/C)^2+\bar{\omega}^2(R+N\bar{r})^2]^{1/2}} \tag{20}$$

and

$$\cos\alpha=\frac{L\bar{\omega}^2-1/C}{[(L\bar{\omega}^2-1/C)^2+\bar{\omega}^2(R+N\bar{r})^2]^{1/2}}, \tag{21}$$

where $-\pi/2\leqslant\alpha\leqslant 0$.

IV. ANALYSIS OF THE KURAMOTO MODEL

Equation (4) is a variation of the Kuramoto model studied by Sakaguchi and Kuramoto [15], who analyzed the problem using a self-consistency approach. First, one introduces a complex order parameter

$$\sigma e^{i\psi}=\frac{1}{N}\sum_{k=1}^{N} e^{i\theta_k}, \tag{22}$$

which is a useful measure of the phase coherence of the dynamical state. For instance, $\sigma=0$ corresponds to an incoherent state, whereas $\sigma=1$ for perfect in-phase locking. For a symmetric, unimodal bare frequency distribution $g(\omega)$ and in the large-N limit, numerical simulations indicate that σ settles down to a constant value and ψ rotates uniformly, with $\psi=\Omega t$. Thus Ω represents the mutual locking frequency, which in general differs from the mean bare frequency $\bar{\omega}$.

We can readily determine which set of oscillators mutually lock. Upon multiplying Eq. (22) by $e^{-i(\theta_j+\alpha)}$ and taking the imaginary part, we can rewrite Eq. (4) as

$$\dot{\theta}_j=\omega_j-K\sigma\,\sin(\theta_j-\psi+\alpha). \tag{23}$$

Using variables in a rotating frame defined by $\varphi_j=\theta_j-\Omega t$, this equation becomes

$$\dot{\varphi}_j=\omega_j-\Omega-K\sigma\,\sin(\varphi_j+\alpha). \tag{24}$$

Thus the jth oscillator locks to the frequency Ω provided $|\omega_j-\Omega|\leqslant K\sigma$. In the infinite-$N$ limit, the fraction f of locked oscillators is

$$f=\int_{\Omega-K\sigma}^{\Omega+K\sigma} d\omega\, g(\omega). \tag{25}$$

What about the oscillators that do not lock? Equation (24) can be explicitly integrated and one finds that each drifting oscillator winds at a dressed frequency $\tilde{\omega}_j$ given by

$$\tilde{\omega}_j^2=(\omega_j-\Omega)^2-(K\sigma)^2. \tag{26}$$

For the order parameter to remain constant in the rotating frame (as assumed), it is necessary to impose the further condition that the drifting oscillators arrange themselves in a stationary distribution around the circle. The story of how this comes about (and in what sense it is true) is an interesting one [14,28], but here we simply assume its validity.

By solving for the stationary density of these drifting oscillators, along with the phase positions of the locked oscillators, and then substituting the results into the definition (22), one arrives at the self-consistency relation [15]

$$\sigma e^{i\alpha}=K\sigma\left(iJ+\int_{-\pi/2}^{\pi/2} d\xi\; g(\Omega+K\sigma\,\sin\xi)\; e^{i\xi}\cos\xi\right), \tag{27}$$

where

$$J=\int_0^{\pi/2} d\xi\,\frac{\cos\xi(1-\cos\xi)}{\sin^3\xi}[g(\Omega+\mu)-g(\Omega-\mu)] \tag{28}$$

and $\mu=K\sigma/\sin\xi$. Given the parameters of the problem, namely, K, α, and the function $g(\omega)$, this equation can be solved to yield the desired quantities σ and Ω, which in turn allows one to compute the fraction of locked oscillators via Eq. (25).

There is always the trivial solution $\sigma=0$, corresponding to a completely desynchronized state. But for K large enough, there is also a nontrivial solution with $\sigma>0$. Typically one needs to solve Eq. (27) numerically. For example, suppose one wants to map out the nonzero solution branch as a function of the width Δ of the given bare frequency distribution. An efficient scheme is to start with a very small value of Δ, so that practically all the junctions are locked and the corresponding solution (Ω,σ) lies very close to the initial guess $(\bar{\omega},1)$. The precise solution can be determined by using, e.g., Newton's method for computing the zeros of functions. Then one can follow the solution branch from there by slowly increasing the width Δ, using the most recently calculated values of Ω and σ as the initial guess for the next case. Notice also that the numerical integration on the right-hand side of Eq. (27) may require special care if Δ is very small.

V. COMPARISON WITH NUMERICAL SIMULATIONS

Having established the connection with the Kuramoto model, we are in a position to make quantitative predictions about the dynamical transitions in the Josephson array. As a first example we consider an array of $N=100$ with disorder in the junction critical currents only. Figure 3 shows the fraction of locked junctions versus the spread Δ in critical currents. The critical currents were chosen to match a normalized parabolic distribution with mean $\bar{I}$ and full width 2Δ:

$$P(I)=\frac{3}{4\Delta^3}[\Delta^2-(I-\bar{I})^2]. \tag{29}$$

The other parameter values are listed in the figure caption. For these parameter values, one calculates from Eqs. (20) and (21) the corresponding Kuramoto parameters $K=0.0601$ and $\cos\alpha=0.3878$. The solid curve is then generated by solving Eqs. (27) and (25) for each value of Δ. The open circles are the results from direct numerical simulations of the original circuit equations (1) and (2). The agreement is very good.

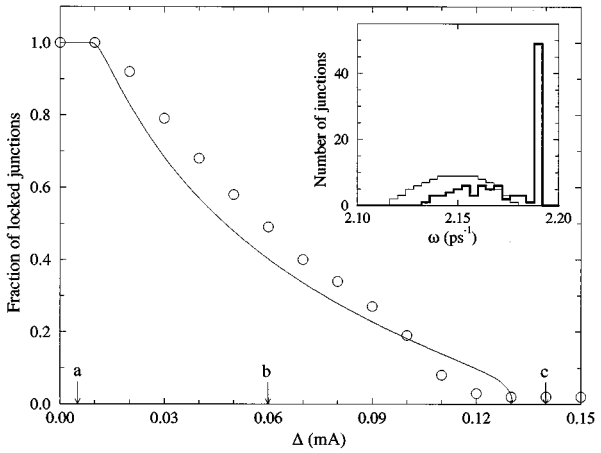

FIG. 3. Fraction of junctions locked to a common frequency as a function of the spread Δ of critical currents for $N=100$, $I_B=1.5$ mA, $R=50\ \Omega$, $L=25$ pH, $C=0.04$ pF, $\bar{I}=0.5$ mA, and all junctions $r_i=0.5\ \Omega$. Circles correspond to numerical simulations of Eqs. (1) and (2). The solid line corresponds to Eq. (25). Power spectra for regimes a–c are shown in Fig. 4. The inset shows histograms for the bare (thin line) and dressed (thick line) frequencies at the point $\Delta=0.06$ mA.

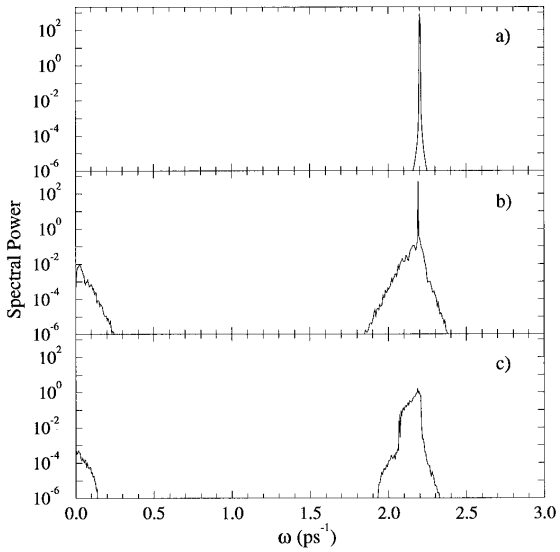

FIG. 4. Power spectra (in arbitrary units) for the ac component of the total array voltage $(\hbar/2e)(\Sigma\dot{\phi}_k-\langle\Sigma\dot{\phi}_k\rangle)$, where angular brackets indicate time average, for the three different regimes of Fig. 1: (a) $\Delta=0.005$ mA, (b) $\Delta=0.06$ mA, and (c) $\Delta=0.14$ mA.

We see that there are three different dynamical regimes. As the disorder is decreased from a large value, there is a transition at $\Delta=\Delta_c$ signaling the onset of frequency locking; for $\Delta_L<\Delta<\Delta_c$ there is partial frequency locking; for $\Delta<\Delta_L$ the frequency locking is complete. The inset shows the distribution of bare and dressed frequencies at $\Delta=0.06$ mA, where about half of the junctions are locked.

Each transition is accompanied by a distinctive signature in the power spectrum for the total voltage across the array. As Δ is lowered below Δ_L the power spectrum develops a sharp line at the locking frequency Ω (and its harmonics), while at $\Delta=\Delta_c$ the broadband spectrum is completely quenched. These features are readily apparent in Fig. 4, which shows the results of numerical simulations for three values of Δ corresponding to the labeled a,b,c in Fig. 3. In principle, the addition of thermal noise can wash out these sharp freatures; however, we have run simulations including Johnson noise generated by both junction and load resistances for a temperature of 4 K and the spectra in Fig. 4 are essentially unchanged except for the presence of a flat noise floor at 10^{-5}.

We consider as a next example a situation more natural for real experiments, where the bias current I_B is used as the control parameter rather than the disorder level Δ. Varying I_B simultaneously affects all of the Kuramoto parameters ω_j, K, and α. As I_B is decreased from a large value, the effective coupling strength $K\cos\alpha$ passes through a maximum as shown in Fig. 5. As a result, the effective coupling strength may never be strong enough to induce complete locking.

Figure 6 shows the results for two levels of intrinsic disorder, plotting the fraction of frequency locked junctions vs I_B. For these runs, the junction critical currents I_j were chosen to match Eq. (29) as before, but the product $I_j r_j$ was the same for all junctions, a situation more typical of disorder in superconductor-normal-superconductor arrays [29]. Note that for a given Δ, keeping the product $I_j r_j$ constant increases the spread in bare frequencies and so increases the effective disorder. Once again, we see that the predictions based on the Kuramoto model agree quite well with the numerical simulations. Note that for the larger disorder case shown, $\Delta=0.002$ mA (asterisks), complete frequency locking is never achieved. Even so, for somewhat larger critical currents (e.g., 2 mA) full locking is seen at larger values of $\Delta/\bar{I}$ (e.g., 2%). This is in the range of present fabrication techniques [25].

We turn next to an issue concerning experimental observation. Although recent developments have made it possible to directly image and identify mutually locked junctions [30], a more standard alternative is to measure the frequency spectrum of the total voltage across the load. As mentioned earlier, the onset of order is signaled by the birth of a narrow line at frequency Ω [compare Figs. 4(b) and 4(c)]. We can calculate an explicit expression for the strength A_Ω of this line from the Kuramoto model as follows.

According to Eq. (15), the load current $Q(t)$ is

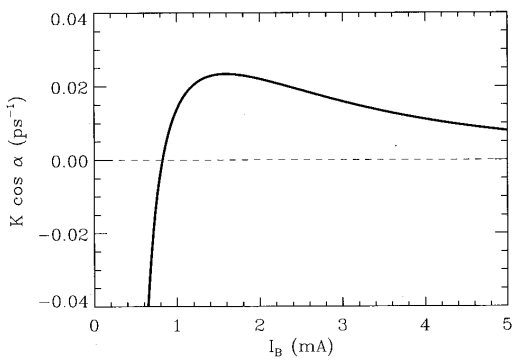

FIG. 5. Typical dependence of the effective coupling strength $K\cos\alpha$ vs bias current I_B.

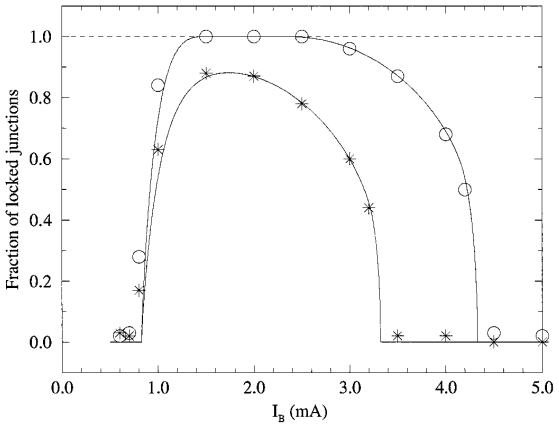

FIG. 6. Fraction of locked junctions f vs bias current I_B, for $N=100$, $R=50\ \Omega$, $L=25$ pH, $C=0.04$ pF, $\bar{I}=0.5$ mA, and $\bar{r}=0.5\ \Omega$. The solid lines correspond to Eq. (25). The symbols correspond to numerical simulations of Eqs. (1) and (2), circles for $\Delta=0.001$ mA and asterisks for $\Delta=0.002$ mA.

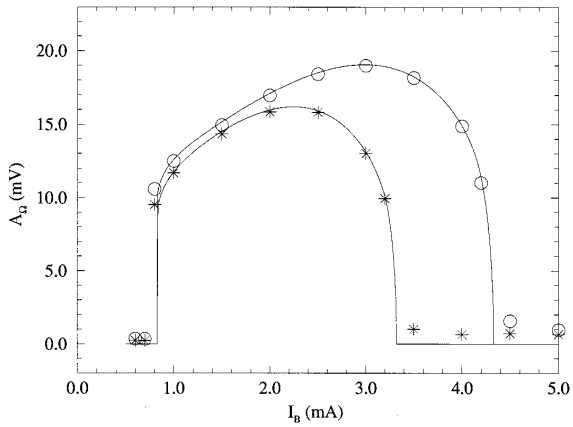

FIG. 7. Dependence of A_Ω vs the bias current I_B, for the same parameters shown in Fig. 6. The solid lines correspond to Eq. (35), the symbols to numerical simulations of Eqs. (1) and (2).

$$Q(t)=\sum_n B_n \sum_k \cos[n\theta_k(t)+\beta_n]. \tag{30}$$

Using $\alpha=-\pi-\beta_1$, the fundamental ($n=1$) component Q_1 can be written as

$$Q_1(t)=-B_1\sum_k \cos[\theta_k(t)-\alpha]. \tag{31}$$

By definition of the order parameter (22), we have

$$Q_1(t)=-NB_1\sigma\cos(\psi-\alpha) \tag{32}$$

or, using the Kuramoto ansatz $\psi=\Omega t$, the load current is

$$\dot{Q}_1(t)=NB_1\sigma\Omega\sin(\Omega t-\alpha). \tag{33}$$

The voltage drop V across the array is directly related to the load current by the load circuit equation $V=L\ddot{Q}+R\dot{Q}+Q/C$. Thus the fundamental component of the voltage V_1 is given by

$$V_1(t)=A_\Omega\sin(\Omega t+\gamma-\alpha), \tag{34}$$

where the amplitude is

$$A_\Omega=2K\sigma\frac{I_B^2-\bar{I}^2}{\bar{\omega}^2\bar{I}}\sqrt{(L\Omega^2-1/C)^2+\Omega^2R^2} \tag{35}$$

and the dephasing γ is given by

$$\cos\gamma=\frac{L\Omega^2-1/C}{\sqrt{(L\Omega^2-1/C)^2+\Omega^2R^2}}. \tag{36}$$

Figure 7 shows the results of simulations for the same set of circumstances as Fig. 6, except now A_Ω is plotted as a function of I_B. The agreement between simulations and the predicted behavior is once again very good. The shape of the A_Ω-I_B curves is very similar to that of the corresponding f-I_B curves. The main difference is that A_Ω shows no dramatic change at the complete-locking transition; consequently, for this transition it is better to monitor the broadband low-frequency part of the voltage output, which is quenched at this transition [compare Figs. 4(a) and 4(b)]. On the other hand, since A_Ω is directly proportional to σ [cf. Eq. (35)] it is a good order parameter for determining the onset of coherence.

Finally, we note that the power delivered to a matched load at frequency Ω is given by $P_\Omega=fA_\Omega^2/2R$, which for these parameters is about 30 nW per junction. This should be sufficient power to detect using on-chip measurements.

ACKNOWLEDGMENTS

We thank Sam Benz for numerous helpful discussions on the physics of Josephson junction arrays. Research was supported in part by the ONR under Contract No. N00014-J-1257, NATO Collaborative Research Grant No. CRG-950282, NSF Grants Nos. DMS-9057433 and DMS-9500948, and DGICYT (Spain) Grant No. PB94-1167.

[1] T. van Duzer and C. W. Turner, *Principles of Superconductive Devices and Circuits* (Elsevier, New York, 1981).

[2] A. Barone and G. Paterno, *Physics and Applications of the Josephson Effect* (Wiley, New York, 1982).

[3] A. Jain, K. K. Likharev, J. E. Lukens, and J. E. Savageau, Phys. Rep. **109**, 310 (1984).

[4] K. K. Likharev, *Dynamics of Josephson Junctions and Circuits* (Gordon and Breach, New York, 1986).

[5] For this and other topics of recent interest see Proceedings of the ICTP Workshop on Josephson Junction Arrays, edited by H. A. Cerdeira and S. R. Shenoy, special issue of Physica B **222** (4), 253 (1996), and references therein.

[6] C. A. Hamilton, C. Burroughs, and K. Chieh, J. Res. Natl. Inst. Stand. Technol. **95**, 219 (1990).

[7] E. Terzioglu and M. R. Beasley, IEEE Trans. Appl. Supercond. **5**, 3349 (1995); B. Yurke, M. L. Roukes, R. Movshov-

ich, and A. N. Pargellis, Appl. Phys. Lett. **69**, 3078 (1996).
[8] S. Han, B. Baokang, W. Zhang, and J. E. Lukens, Appl. Phys. Lett. **64**, 1424 (1994); P. A. A. Booi and S. P. Benz, *ibid.* **68**, 3799 (1996).
[9] A. T. Winfree, *The Geometry of Biological Time* (Springer, New York, 1980).
[10] S. H. Strogatz and I. Stewart, Sci. Am. (Int. Ed.) **269** (6), 102 (1993).
[11] C. Huygens, XI J. Scavants, 79, 16 March 1665; XII J. Scavants, 86, 23 March 1665.
[12] A. T. Winfree, J. Theor. Biol. **16**, 15 (1967).
[13] Y. Kuramoto, in *Proceedings of the International Symposium on Mathematical Problems in Theoretical Physics*, edited by H. Araki, Lecture Notes in Physics Vol. 39 (Springer, Berlin, 1975); *Chemical Oscillations, Waves, and Turbulence* (Springer, Berlin, 1984).
[14] For a review see S. H. Strogatz, in *Frontiers in Mathematical Biology*, edited by S. Levin, Lecture Notes in Biomathematics Vol. 100 (Springer, Berlin, 1994).
[15] H. Sakaguchi and Y. Kuramoto, Prog. Theor. Phys. **76**, 576 (1986).
[16] S. H. Strogatz, R. E. Mirollo, and P. C. Matthews, Phys. Rev. Lett. **68**, 2730 (1992).
[17] S. H. Strogatz and R. E. Mirollo, J. Stat. Phys. **63**, 613 (1991).
[18] L. L. Bonilla, J. C. Neu, and R. Spigler, J. Stat. Phys. **67**, 313 (1992).
[19] J. L. van Hemmen and W. F. Wreszinski, J. Stat. Phys. **72**, 145 (1993).
[20] J. D. Crawford, J. Stat. Phys. **74**, 1047 (1994); Phys. Rev. Lett. **74**, 4341 (1995).
[21] H. Daido, Prog. Theor. Phys. **88**, 1213 (1992); Phys. Rev. Lett. **73**, 760 (1994).
[22] H.-A. Tanaka, A. J. Lichtenberg, and S. Oishi, Physica D **100**, 279 (1997).
[23] K. Wiesenfeld, P. Colet, and S. H. Strogatz, Phys. Rev. Lett. **76**, 404 (1996).
[24] See, e.g., P. Hadley and M. R. Beasley, Appl. Phys. Lett. **50**, 621 (1987).
[25] P. A. A. Booi and S. P. Benz, Appl. Phys. Lett. **64**, 2163 (1994).
[26] J. W. Swift, S. H. Strogatz, and K. Wiesenfeld, Physica D **55**, 239 (1992).
[27] K. Wiesenfeld and J. W. Swift, Phys. Rev. E **51**, 1020 (1995).
[28] P. C. Matthews, R. E. Mirollo, and S. H. Strogatz, Physica D **52**, 293 (1991).
[29] S. P. Benz, Appl. Phys. Lett. **67**, 2714 (1995).
[30] S. G. Lachenmann, T. Doderer, D. Hoffmann, R. P. Huebener, P. A. A. Booi, and S. P. Benz, Phys. Rev. B **50**, 3158 (1994); S. G. Lachenmann, T. Doderer, and R. P. Huebener, *ibid.* **53**, 14 541 (1996).